Journal of Biomechanical Science and Engineering

Vol. 7, No. 2, 2012

Modeling of Viscoelastic and Nonlinear Material Properties of Liver Tissue using Fractional Calculations*

Yo KOBAYASHI**, Atsushi KATO***, Hiroki WATANABE***,
Takeharu HOSHI***, Kazuya KAWAMURA** and Masakatsu G. FUJIE**

** Faculty of Science and Engineering, Waseda University,
59-309, 3-4-1 Ohkubo, Shinjuku-ku, Tokyo 169-8555, Japan
E-mail: you-k@fuji.waseda.jp

*** Graduate School of Science and Engineering, Waseda University,
59-309, 3-4-1 Ohkubo, Shinjuku-ku, Tokyo 169-8555, Japan

Abstract

We present a material model to represent the viscoelastic and material, nonlinear properties of liver tissue for needle insertion simulation. Material properties of liver tissue were measured using a rheometer and modeled from the measured data. The liver viscoelastic characteristics were represented by differential equations, including the fractional derivative term. Next, nonlinearity with respect to the fractional derivative was measured, and the stress–strain relationship using a cubic function was modeled. The material properties of liver tissue were represented by a simple equation with only a few parameters. We evaluated the variety of each stiffness parameter from measurements of 50 samples. The results showed a high degree of variation in each stiffness parameter, especially with respect to nonlinearity. Moreover, each parameter had a low correlation coefficient. We also modeled the probability of variation in material properties from these results to provide a basis for deformation simulations considering individual patient differences.

Key words: Liver, Viscoelasticity, Stress–Strain Relationship, Material Properties, Nonlinearity

1. Introduction

Recent research and development has been performed on surgical robots and navigation systems to achieve more minimally invasive and precise surgery (1)–(4). Therapies using needle insertion, such as radio frequency ablation, have become a major method for cancer treatment. Cancer existing inside the liver can be necrotized by delivering a needle tip to the cancer for injection of ethanol into the tumor (percutaneous ethanol injection therapy) or for tumor ablation (radio ablation therapy). Research into robotic systems to assist needle insertion has also been conducted to improve the accuracy of needle placement and expansion of the approach path (5)–(8).

In percutaneous therapy, it is necessary to accurately place the needle tip into the target cancer. Because target organs such as the liver consist of soft tissue, the organ morphology can deform upon needle insertion and change the position of the target lesion. Moreover, the needle path is limited to a straight line in many percutaneous therapies because the path is constrained by the abdominal wall. For these reasons, it is necessary to devise a strategy

*Received 21 Apr., 2011 (No. 11-0261)
[DOI: 10.1299/jbse.7.177]

that accounts for organ deformation caused by the needle insertion.

A numerical simulation of needle insertion in a virtual surgery environment reproduced with physical models of organs is a useful research tool. The needle must be accurately directed to the target lesion upon entering the tissue, because the needle punctures and advances in the tissue immediately. Therefore, it is important to make a correct analysis of organ deformation and to determine the appropriate conditions at the point of puncture.

Many studies have researched the measurement and modeling of material properties of living tissue. For example, Miller and colleagues presented three-dimensional (3D), nonlinear, viscoelastic constitutive models for the liver, kidney (9) and brain tissue (10). Gao et al. (11) researched the nonlinear material properties and proposed a constitutive model of the material properties of liver. Liu et al. (12) developed a nonlinear viscoelastic model to represent the material properties based on a stress relaxation test. Sakuma et al. (13)(14) derived an equation that combines both logarithmic and polynomial strain energy forms of pig liver from combined compression and elongation tests. Additionally, Kerdok et al. (15) used a generalized Voigt model for perfused ex vivo porcine liver. Finally, Kim et al. (16) conducted tests and modeled porcine liver using the Kelvin model.

These models represent either nonlinear properties or viscoelastic properties. Only one study reported both the nonlinear and viscoelastic modeling of living tissue (17). However, the equation to represent such a model is very complex and has many parameters. Moreover, the variation in parameters due to individual differences has not been quantified, even though the differences in the parameters greatly affect the simulation results.

The objective of our research was to construct a viscoelastic and nonlinear model based on detailed material data measured from in vitro hog liver. We focused on the modeling of the material properties of liver and representation of the properties by a simple equation with only a few parameters. Table 1 summarizes recent/relevant models and numbers of parameters, including the model developed in this study.

2. Viscoelastic properties

2.1 Test conditions

We used a rheometer (AR550, TA Instruments) to measure the torque loaded on the sample and the torsional angle of the sample (Fig. 1). The shear modulus of the sample was then calculated based on these results. We used hog liver in the present study because porcine abdominal organs have mechanical properties similar to those of humans. The liver was cut into a circular, cylindrical shape (ϕ20 mm, height 5 mm) and placed on a measurement table. We used cryogenically preserved liver samples that were taken within 24 h of death and which did not include membrane or large blood vessels. Specimens were not frozen at any time during the procedure. The condition for each test environment involved soaking test samples in normal saline solution at a temperature of 36 °C. The normal saline solution was stable and there was no reflux flow. Sandpaper was attached to the top plate and the measurement table to prevent sliding. The mean stress and strain values on the liver sample are referred to in the experimental results, because they are adequate for consideration of the nonlinear properties in Section 3.

2.2 Methods

1) Dynamic viscoelastic test: We used mechanical impedance shown in Eq. (1) to represent the dynamic viscoelastic test results.

$$G^* = G' + jG'' \qquad (1)$$

where G^* is the complex shear modulus; G' is the storage elastic modulus, and G'' is the loss elastic modulus. G' and G'' model the viscoelastic properties of the liver.

Table 1 Summary of recent/relevant models and number of parameters

Paper	Model name	Number of parameters (viscoelasticity)	Number of parameters (viscoelasticity & nonlinearity)
This paper		2	4
Fung et al. [18]	Maxwell model	2	No nonlinearity
Fung et al. [18]	Voigt model	2	No nonlinearity
Kim et al. [16]	Kelvin model	3	No nonlinearity
Liu et al. [12]	Dual Maxwell model	4	10
Kerdok et al. [15]	Generalized Voigt model	5	No nonlinearity

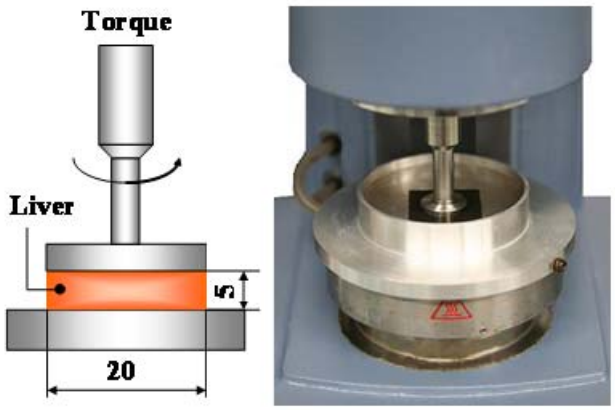

Fig. 1 Measurement equipment (rheometer)

The sine-wave stress from 0.1 to 200 rad/s, providing 3% strain amplitude, was loaded on the liver sample described in Section 2.1. The mechanical impedance of the hog liver was obtained in each frequency.

2) Creep test: The creep test, including a stress of 150 Pa, was performed on the liver sample. The time series data of strain were measured during the experiment.

2.3 Results

1) Dynamic viscoelastic test: The experimental results of mechanical impedance of the liver are shown in Fig. 2(a) and are represented by a log-log diagram. Both the storage elastic modulus *G'* and the loss elastic modulus *G"* increased as the frequency increased.

2) Creep test: As shown in Fig. 3, the strain of the liver sample increased over a time interval of 180 s. From 0-2 s, the strain vibrated in the early stage of the creep experiment.

2.4 Modeling

1) Dynamic viscoelastic test: In general, a needle is inserted into an organ at a low velocity; hence, the response is mainly affected by low-frequency characteristics. Therefore, the frequency band was set from 0.1 to 10 rad/s. As shown in the log–log diagram of Fig. 2(a), the storage elastic modulus *G'* increased proportionally. The loss elastic modulus *G"* also increased proportionally, since the slopes of *G'* and *G"* were nearly the same. *G'* and *G"* are presented by Eqs. (2) and (3), respectively.

$$\log G' = k \log(\omega) + \log(G'_0) \quad (2)$$

$$\log G'' = k \log(\omega) + \log(G''_0) \quad (3)$$

The following Eqs. (4) and (5) were derived from (2) and (3), respectively.

$$G' = G'_0 \, \omega^k \quad (4)$$

$$G'' = G''_0 \, \omega^k \quad (5)$$

Thus, the mechanical impedance is provided by (6).

$$G^* = G(j\omega)^k \quad (6)$$

where G is the viscoelasticity and has the following relationship:

$$G = \sqrt{G_0^{'2} + G_0^{''2}} \quad (7)$$

$$G'_0 = G\cos(\frac{\pi}{2}k) \quad (8)$$

$$G''_0 = G\sin(\frac{\pi}{2}k) \quad (9)$$

In the above equations, G represents the magnitude of elastic and viscous properties, because k presents a material index from 0 (elastic) to 1 (viscous). The viscoelastic characteristics of the liver are provided using differential Eq. (10) derived from the mechanical impedance of (6).

$$G\frac{d^k\gamma}{dt^k} = \tau \quad (10)$$

where G is the viscoelasticity, γ the strain, τ the stress, and t is time.

The derivative order k was set equal to 0.1 based on the slope of G' and G'' in Fig. 2(a). Consequently, we were able to model the viscoelastic properties of the liver using a fractional derivative that represented a derivative of non-integer orders. The mechanical impedance of the model by the fractional derivative term is also shown in Fig. 2(a).

2) Creep test: The steady state of the step response following sufficient elapsed time exhibited low-frequency characteristics and is shown by Eq. (11). Equation (10) becomes (11) if (10) is solved for the conditions of the creep test. Here, the loaded stress is constant.

$$\gamma = \frac{\tau_c}{G\,\Gamma(1+k)}t^k = \gamma_c t^k \quad (11)$$

where γ is strain; τ_c is constant stress; G is viscoelasticity, Γ is the gamma function; γ_c is the coefficient deciding the strain value, and t is time. In this case, the Riemann-Liouville definition (12) was used to solve the fractional integration of (10).

$$\mathrm{D}^{-k} f(t) = \frac{1}{\Gamma(k)}\int_0^t (t-\xi)^{k-1} f(\xi) d\xi \quad (12)$$

Equation (11) shows that the steady state of the creep test is provided by the power of time. The model response of the creep test and its power approximation are shown in Fig. 3 (a) and (b).

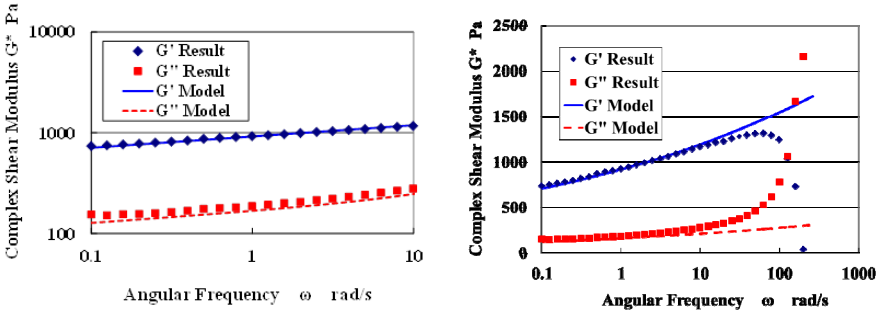

(a) (b)

Fig. 2 Mechanical impedance of the liver. G^* is the complex shear modulus; G' is the storage elastic modulus, and G'' is the loss elastic modulus. The red and blue plots are the experimental results, and the red and blue lines are the responses of our model for (a) over the range of 0.1–10 rad/sec (b) over 10 rad/sec for the vibration of creep test (ref: Fig.3 (b)).

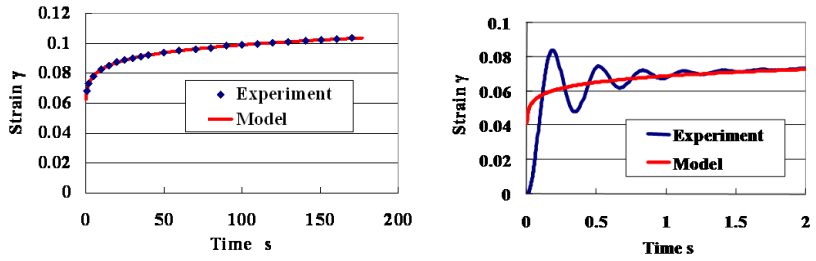

(a) (b)

Fig. 3 (a) Creep test results showing that the strain of the liver sample increased over a time interval of 180 s. The blue plot shows the experimental results, and the red line is the response of our model. (b) Creep test results showing that the model response did not closely represent the vibration of the experimental result. The blue line shows the experimental results. The red line is the model response.

3. Nonlinear properties

3.1 Methods

Nonlinear characteristics of the liver were investigated based on a series of repeated creep tests. The viscoelasticity G, strain γ_c and derivative order k for each stress τ_c were calculated to fit Eq. (11). The test conditions were the same as described in Section 2.1.

3.2 Results

The coefficient of determination R^2 exceeded 95% for each stress. Figure 4 shows the relationship between the applied stress τ_c and strain γ_c, and displays the relationship between the applied stress τ_c and viscoelasticity G.

3.3 Modeling

Figure 4 shows that liver tissue with a low strain of less than approximately 0.2 displayed linear characteristics and a viscoelasticity G at a constant 200 Pa. However, liver with a low strain of more than approximately 0.2 displayed nonlinear characteristics and an increased degree of viscoelasticity G. We modeled the viscoelasticity strain dependence based on these results, using the quadratic function of strain shown by Eq. (13). Next, the stress-strain relationship was modeled using the cubic function described in Eq. (14). Figure

4 also displays the nonlinear properties of the model. As shown, the model described by Eqs. (13) and (14) is sufficient to express nonlinear characteristics.

$$G(\gamma)=\begin{cases} G_o & (\gamma<\gamma_0) \\ G_0(1+a_\gamma(\gamma-\gamma_0)^2) & (\gamma>\gamma_0) \end{cases} \quad (13)$$

$$\tau=\begin{cases} G_o\gamma & (\gamma<\gamma_0) \\ G_0(1+a(\gamma-\gamma_0)^2)\gamma & (\gamma>\gamma_0) \end{cases} \quad (14)$$

where G_o is the linear shear modulus with low strain; γ_0 is the strain in which the characteristics of the liver change to show nonlinearity, and a_γ is the coefficient deciding the change in stiffness.

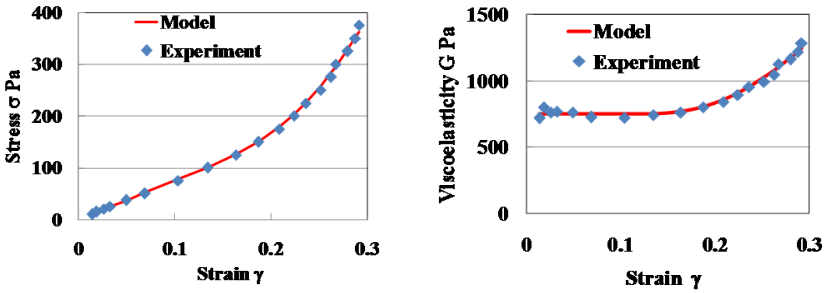

(a) (b)

Fig. 4 Relationships of (a) stress-strain and (b) stress-viscoelasticity. Stress is computed by multiplying viscoelasticity by strain (as represented by the same properties in the figures). Both figures show that the liver tissue displays high nonlinearity. Specifically, liver tissue with a low strain of more than approximately 0.2 displayed nonlinear characteristics and an increased degree of viscoelasticity *G*. From this result, we modeled the material nonlinear properties of the liver tissue by Eqs. (13) and (14).

4. Evaluation of parameter variations

Human tissue has large individual differences, making material parameters inherently uncertain. When incorporating simulation results into clinical practice, it is crucial to evaluate the individual variability of the organ tissue under investigation. This section describes the evaluation of parameter variances in the proposed model.

4.1 Method

Measurements of the nonlinear stiffness parameters described in Section 3 were repeatedly performed on 50 hog liver samples. The viscoelastic properties *k* were also measured by dynamic viscoelastic tests described in Section 2. Next, histograms of the data were created to visualize the distribution status of G_o, a_γ and *k*, while a histogram hierarchy was calculated from a total of 50 data via the Sturges' formula.

4.2 Results

Figure 5 shows the viscoelasticity *G* vs. the strain γ_c diagram of the 50 sample livers. The histograms of G_o, a_γ and γ_0 in Eq. (13) and of *k* in Eq. (10) are shown in Fig. 6. Key parameter values, such as the mode, maximum and minimum values of each parameter, are shown in Table 2. We investigated the variation in the parameters using normal probability distribution described in Eq. (16).

$$f_{Normal}(x) = \frac{1}{\sqrt{2\pi}\sigma} e^{-\frac{(x-\mu)^2}{2\sigma^2}} \qquad (16)$$

where f_{normal} is probability density function, σ is variance, x is random variable, and μ is mean. Figure 6 also displays the probability distribution of G_o, a_γ, γ_0 and k, respectively.

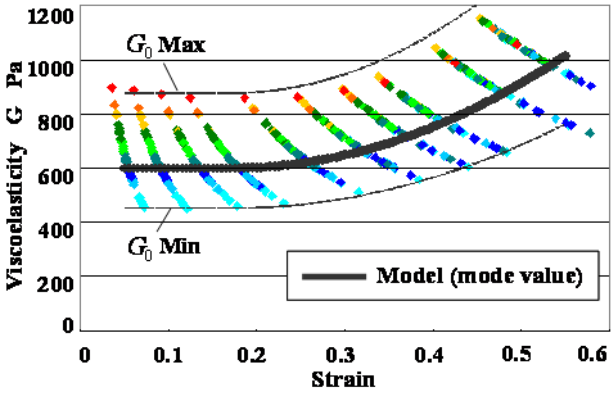

Fig.5 Variation in nonlinear properties. Each color of the plot indicates data from a specific hog liver. The experimental results show significant variations. For this reason, we have plotted two curves; one using the mode value of γ_o and a_γ and the maximum value of G_o, the other using the mode value of γ_o and a_γ and the minimum value of G_o. Almost all of the plots are between the two curves.

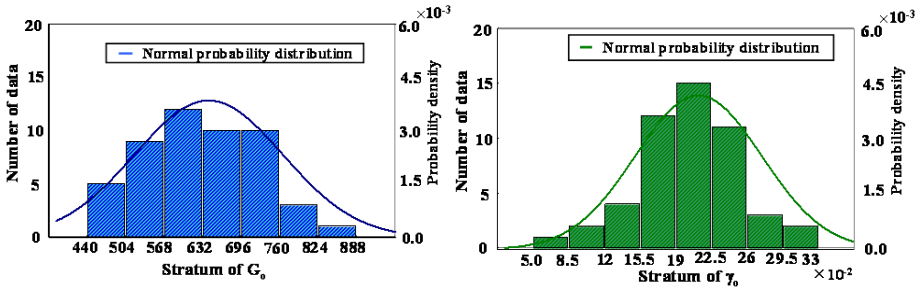

Fig. 6 Histogram of stiffness parameters. Each interval was divided by the magnitude of the parameters (G_o, a_γ, γ_0, k). The height of the rectangle in each interval presents the data number and probability density within that interval. These results indicate that the parameters with respect to nonlinearity (a_γ and γ_0) exhibited large variations compared to the parameters with respect to viscoelasticity (G_o, k).

Table 2 Value of each parameter

	G_o [Pa s^k]	a_γ	γ_0	K
Average	637	5.2	0.17	0.126
Variance σ^2	9136	3.0	$2.5*10^{-3}$	$1.4*10^{-4}$
Minimum value	456	1.9	0.05	0.118
Maximum value	875	9.7	0.29	0.135
Mode	626	4.8	0.17	0.127
Standard derivation	96	1.7	0.05	$3.8*10^{-3}$
Kurtosis	-0.26	0.38	0.62	-0.35
Skewness	0.18	0.44	0.05	0.28

5. Discussion

1) Model using the fractional derivative: The fractional model described in Eq. (10) is sufficient to express the viscoelastic characteristics of the liver when ω is lower than 10 rad/s as shown in Fig.2 (a). Viscoelastic materials, whose behaviors are dependent on elastic and viscous components, have been modeled by combinations of springs and dashpots, as in the Voigt (spring and dashpot in series), Maxwell (spring and dashpot in parallel) and Kelvin (spring in parallel with a Maxwell) models. However, models such as these cannot represent the viscoelastic properties shown in Fig. 3 (a) by a simple term. Some studies have modeled the viscoelastic properties using a generalized Maxwell-Weichert model, which has many spring-dashpot Maxwell elements. The existing models indicate that the representative equation is very complex and involves an excessive number of material parameters. In contrast, fractional models have successfully been fitted to experimental data within a broad frequency range using only two parameters, G and k, as shown in (10). In modeling biomaterials, a modeling method using the fractional derivative approach is more suitable than a method using a combination of elastic and viscous elements. Equations (4) and (5) belong to a more general description called power laws. However, it is difficult for only this power law description to be used in the actual application, because the calculation method of the equation is not established, and it results in a calculation error and/or a long calculation time. The calculation method of fractional derivative description is superior in accuracy and calculation time. The generality of the modeling is low because the derivative description is not appropriate, i.e., when k is different for G' and G''. In this study, we proposed modeling using a fractional derivative description for superiority in actual application, because the dynamic viscoelastic test results displayed the same value in k for G' and G''.

2) Viscoelasticity of the fractional derivative: Equation (10) represents the elastic element if the derivative order is $k = 0$, and the viscous element if the derivative order is $k = 1$. Therefore, the fractional derivative model has intermediate properties between the elastic body and viscous body. As such, the derivative order k represents the degree of viscosity of the system in the fractional derivative model. A viscoelastic material is more governed by elastic properties than by the viscous properties when the derivative order k is close to 0, whereas a viscoelastic material is more governed by viscous properties than by elastic properties when the derivative order k is close to 1. The value of the derivative order k was 0.1 from the experimental result displayed in Fig. 2(a), indicating that the steady-state characteristics of liver are intermediate between the elastic and viscous bodies.

3) Creep experiment: In the experimental results, the strain of the liver continually expanded over 180 s. Representing continual expansion over a long term is difficult by basic models such as the Voight model. The Maxwell model is able to represent long-term

expansion, but only expands linearly. Figure 3 (a) shows that the model response effectively indicates the steady state of the actual liver creep test. In fact, the coefficient of determination, R^2, exceeded 95% in Fig. 3 (a). The fractional derivative easily represents the continual expansion over a long time with one differential term. In Fig. 3 (a), the model response did not closely represent the vibration of the experimental result. The vibration occurred because of the effect of high frequencies beyond 10 rad/s (ref. Fig.2 (b): the change in the range around 100 rad/sec affects the vibration in the creep test). However, the model response passed through the center of vibration. This result suggests that our model represents low-frequency characteristics effectively, particularly early in the step response. As mentioned above, the needle is generally inserted into the organ at a low velocity; hence, the response is not largely affected by high frequencies. As shown by the vibration phenomenon and the difference with the dynamic viscoelastic test, our fractional model could not cover the high frequency responses of liver. High frequency modeling will be required for applications involving high frequency change.

4) Parameter variations: The maximum values of G_o, a_γ, γ_0 and k were approximately 2, 5, 2 and 1.1 times the minimum values, respectively. These results indicate that the degree of nonlinearity a_γ has a large variation compared with the degree of viscoelastic properties k. According to Table 2, the mode values of G_o, γ_o, a_γ and k are closer to the average values. The kurtosis of G_o was lower than that of the other parameters. According to the histograms in Fig. 6, G_o values contributed to a large mean variance, whereas the values of γ_o, a_γ and k contributed to a low mean variance.

5) Difference with in vivo tissue: it is well known that there is difference in material properties between in vivo tissue and tissue samples. This difference may result from the presence of blood inside vessels that increases internal pressure and causes samples to swell. In our experiment, there was no blood inside the liver sample while the liver samples were soaked in normal saline solution. Therefore, the findings from our experiment may differ with those from an in vivo test. The issue will be further examined in future work.

6. Conclusions

This paper presents a material model to represent viscoelastic and nonlinear properties of liver tissue for needle insertion simulation. First, the material properties of the liver were measured using a rheometer and modeled from the collected data. The liver viscoelastic characteristics were represented by differential equations, including the term of the fractional derivative. Next, nonlinearity in terms of the fractional derivative term was measured. We then modeled the stress–strain relationship using a cube function. Consequently, we developed the material properties of liver tissue, which were represented by a simple equation and a few parameters. Finally, we evaluated the variety of each stiffness parameter from the measurement of 50 samples. The results showed that each stiffness parameter, particularly the parameter related to nonlinearity, had a large variation.

Acknowledgments

This work was supported by the High-Tech Research Centre Project from MEXT (Ministry of Education, Culture, Sports, Science and Technology), the "Establishment of Consolidated Research Institute for Advanced Science and Medical Care", the Encouraging Development Strategic Research Centres Program, the Special Coordination Funds for Promoting Science and Technology, Ministry of Education, Culture, Sports, Science and Technology, Japan, the Global COE (Centres of Excellence) Program “Global Robot Academia”, Waseda University, Tokyo, Japan, the “Robotic Medical Technology Cluster in Gifu Prefecture”, Knowledge Cluster Initiative, Ministry of Education, Culture, Sports, Science and Technology, Japan, and a Grant-in-Aid for Young Scientists (B) (21700513).

References

(1) Intuitive Surgical, available from <http://www.intuitivesurgical.com>, (accessed 2011-04-20).

(2) Hongo, K., Kakizawa, Y., Koyama, J., Kan, K., Nishizawa, K., Tajima, F., Fujie, M. G. and Kobayashi S., Microscopic-Manipulator System for Minimally Invasive Neurosurgery - Preliminary Study for Clinical Application, *Proceedings of the 15th Congress and Exhibition of Computer Assisted Radiology and Surgery*, (2001), pp. 265-269.

(3) Taylor, R. H. and Stoianovici, D., Medical Robotics in Computer-Integrated Surgery, *IEEE Transactions on Robotics and Automation*, Vol. 19 (2003), pp.765−781.

(4) Dario, P., Hannaford, B. and Menciassi, A., Smart Surgical Tools and Augmenting Devices, *IEEE Transactions on Robotics and Automation*, Vol. 19 (2003), pp.782-792.

(5) Kazanzides, P., Fichtnger, G., Hager, G. D., Okamura, A. M., Whitcomb, L. L. and Taylor, R. H., Surgical and interventional robotics, *IEEE Robotics & Automation Magazine*, Vol. 15 (2008), pp.122-130.

(6) Fichtnger, G., Kazanzides, P., Okamura, A. M., Hager, G. D., Whitcomb, L. L. and Taylor, R. H., Surgical and Interventional Robotics: Part II, *IEEE Robotics & Automation Magazine*, Vol. 15 (2008), pp.94-102.

(7) Hashizume, M., Yasunaga, T., Tanoue, K., Ieiri, S., Konishi, K., Kishi, K., Nakamoto, H., Ikeda, D., Sakuma, I., Fujie, M. and Dohi T., New Real-Time MR Image-Guided Surgical Robotic System for Minimally Invasive Precision Surgery, *International Journal of Computer Assisted Radiology and Surg*ery, Vol. 2 (2008), pp.317–325.

(8) Oura, M., Kobayashi, Y., Okamoto, J. and Fujie, M. G., Development of MRI Compatible Versatile Manipulator for Minimally Invasive Surgery, *Proceedings of 2006 IEEE Biomedical Robotics and Biomechatronics*, (2006), pp.176-181.

(9) Miller, K., Constitutive Modelling of Abdominal Organs, *Journal of Biomechanics*, Vol. 33 (2000), pp.367-373.

(10) Miller, K., Chinzei, K., Orssengo, G. and Bednarz, P., Mechanical Properties of Brain Tissue In-Vivo: Experiment and Computer Simulation, *Journal of Biomechanics*, Vol. 33 (2000), pp.1369-1376.

(11) Gao, Z., Lister, K. and Desai, J. P., Constitutive Modeling of Liver Tissue: Experiment and Theory, *Proceedings of 2008 IEEE Biomedical Robotics and Biomechatronics*, (2008), pp.477-482.

(12) Liu, H., Noonan, D. P., Zweiri, Y. H., Althoefer, K. A. and Seneviratne, L. D., The Development of Nonlinear Viscoelastic Model for the Application of Soft Tissue Identification, *2007 IEEE International Conference on Intelligent Robotics and Systems*, (2007), pp.208-213.

(13) Sakuma, I., Nishimura, Y., Chu, C. K., Kobayashi, E., Inada, H., Chen, X. and Hisada, T., In Vitro Measurement of Mechanical Properties of Liver Tissue under Compression and Elongation Using a New Test Piece Holding Method with Surgical Glue, *Proceedings of 2003 International Symposium on Surgery Simulation an Soft Tissue Modeling*, (2003), pp.284-292.

(14) Chui, C., Kobayashi, E., Chen, X., Hisada, T., Sakuma, I., Combined compression and elongation experiments and non-linear modelling of liver tissue for surgical simulation, *Medical and Biological Engineering Computing*, Vol. 42(2006), pp.787-798.

(15) Kerdok, A. E., Ottensmeyer, M. P., Howe, R. D., Effects of perfusion on the viscoelastic characteristics of liver, *Journal of Biomechanics*, Vol. 39 (2006), pp.2221-2231.

(16) Kim, J., Tay, B., Stylopoulos, N., Rattner, D. W., Srinivasan, M. A., Characterization of Intra-Abdominal Tissues from In Vivo Animal Experiment for Surgical Simulation, *Proceedings of 2003 Medical Image Computing and Computer-Assisted Intervention*, (2003), pp.206-213.

(17) Schwartz, J. M., Denninger, M., Rancourt, D., Moisan, C. and Laurendeau, D., Modelling Liver Tissue Properties Using a Non-Linear Visco-Elastic Model for Surgery Simulation, *Medical Image Analysis*, Vol. 9 (2005), pp.103-112.

(18) Fung, Y. C., *Biomechanics: Mechanical Properties of Living Tissues*, (1993), Springer-Verlag.